Title

Implications of warming on western United States landfalling atmospheric rivers and their flood damages

Authors

Rhoades, Alan M
Risser, Mark D
Stone, Dáithí A
et al.

Publication Date

2021-06-01

DOI

10.1016/j.wace.2021.100326

Peer reviewed

Weather and Climate Extremes 32 (2021) 100326

Contents lists available at ScienceDirect

Weather and Climate Extremes

journal homepage: www.elsevier.com/locate/wace

Implications of warming on western United States landfalling atmospheric rivers and their flood damages

Alan M. Rhoades [a,*], Mark D. Risser [a], Dáithí A. Stone [b], Michael F. Wehner [c], Andrew D. Jones [a]

[a] Climate and Ecosystem Sciences Division, Lawrence Berkeley National Laboratory, Berkeley, CA, USA
[b] National Institute of Water and Atmospheric Research, Wellington, New Zealand
[c] Computational Research Division, Lawrence Berkeley National Laboratory, Berkeley, CA, USA

ARTICLE INFO

Keywords:
Atmospheric rivers
Western United States
Climate change
Societal impacts
Detection and attribution
Stabilized warming scenarios

ABSTRACT

Atmospheric rivers (ARs) are critical to the hydrological cycle of the western United States with both favorable and formidable impacts to society based on their landfalling characteristics. In this study, we provide a first-of-its-kind evaluation of how landfalling ARs may respond to several stabilized warming scenarios. To do this we combine a recently developed AR detection workflow with an ensemble of uniform high-resolution (0.25°) Community Earth System Model simulations designed to facilitate detection and attribution of extreme events with global warming. These simulations include a world that might have been in the absence of anthropogenic warming (+0 °C), a world that corresponds to present day warming (+0.85 °C), and several future worlds corresponding to +1.5 °C, +2 °C and +3 °C global warming. We show that warming increases the number of water management relevant landfalling ARs from 19.1 ARs per year at +0 °C to 23.6 ARs per year at +3 °C. Additionally, this warming intensifies the amount of water transported by landfalling ARs resulting in a decrease in the fraction of ARs that are "mostly to primarily beneficial" to water resource management (i.e., 91% of ARs at +0 °C to 78% at +3 °C) and an increase in the fraction of ARs that are "mostly or primarily hazardous" to water resource management (i.e., 2% of ARs at +0 °C to 8% at +3 °C). Shifts in AR character also have important ramifications on flood damages, whereby for every +1 °C of additional warming from present conditions annual average flood damages increase by ~$1 billion. These findings highlight the pragmatic implications of climate mitigation aimed at limiting global warming to under +2 °C.

1. Introduction

The meridional branch of the atmospheric portion of the global hydrologic cycle occurs primarily via filamentary pulses of anomalously high water vapor (Newell et al., 1992). These filamentary structures, seen through fields such as integrated vapor transport (IVT), are now commonly referred to as atmospheric rivers (ARs) (Ralph et al., 2018). The anomalous vapor transported via ARs are critical to the local hydrologic cycle in mid-latitudes as the efficiency (on average, ~30%) of turning water vapor into precipitation is limited (Trenberth et al., 2003) and locally available moisture from evapotranspiration alone is insufficient to generate locally observed precipitation totals (Dirmeyer and Brubaker, 2007). The annual variability in the frequency and intensity of ARs are dictated by the interactions between seasonal variations in sea-surface temperatures, equatorial convection and synoptic-to-mesoscale atmospheric dynamics (Payne and Magnusdottir, 2014; Zhou et al., 2018; Kim et al., 2019), particularly through influences on tropical moisture exports and warm conveyer belts (Ralph et al., 2017). The societal implications of this annual variability is considerable as landfalling ARs are central to both water supply and flood risk in many mid-latitude coastal regions (Dettinger et al., 2011; Gimeno et al., 2014; Lamjiri et al., 2018; Payne et al., 2020).

Anthropogenic climate change is expected to intensify the global hydrologic cycle (Thackeray et al., 2018; Prein and Pendergrass, 2019). However, this intensification will likely alter components of the global hydrologic cycle in different ways as adjustments can occur rapidly to slowly (Allan et al., 2020) and have important energetic constraints (Allen and Ingram, 2002). More specific to ARs, these rapid-to-slow adjustments occur primarily through climate change induced changes to dynamical and/or thermodynamical processes (Payne et al., 2020). Feedbacks that alter thermodynamic processes arise primarily from the Clausius-Clapeyron relationship (i.e., column-integrated water vapor

* Corresponding author.
E-mail address: arhoades@lbl.gov (A.M. Rhoades).

https://doi.org/10.1016/j.wace.2021.100326
Received 2 December 2020; Received in revised form 17 March 2021; Accepted 13 April 2021
Available online 9 May 2021

increases at approximately +7.5%/K (Held and Soden, 2006)) that in turn influences the magnitude and variability of moisture sources that seed ARs. Feedbacks to dynamical processes occur primarily through modifications to AR lifecycles through synoptic to mesoscale changes in the seasonal storm-track location and its variability and through more localized changes in wind speed, direction, and shear. The interaction between these two processes can regionally offset one another (Payne et al., 2020) and lead to more heterogeneous responses that may impact AR families (Fish et al., 2019) or flavors (Gonzales et al., 2019) in different ways. Importantly, the relative strength and interplay between these processes is emissions scenario dependent and will likely differ across various spatiotemporal scales and time horizons of climate change.

The true emissions scenario that the global climate will experience in the coming century is highly uncertain given the nonlinear behavior of human decision making (e.g., policy implementation and technological innovation). To address this, a new subfield of climate science known as detection and attribution has emerged over the last decade and provides a means to isolate the effects of anthropogenic emissions on weather events and/or climate trends (Hannart et al., 2016; Stott et al., 2016; Mitchell et al., 2017; Stone et al., 2019). Detection and attribution presents a unique scientific framework by which to isolate how various emissions scenarios after stabilization may intensify the global hydrologic cycle, or more specific to this study landfalling AR characteristics. Moreover, the current generation of climate models that can be run under centennial-scale emissions scenarios are poor at resolving the filamentary form of ARs and, in particular, the landfall lifecycle of AR characteristics (Dettinger, 2011; Hagos et al., 2015; Rhoades et al., 2020a) which, in turn, muddles the attribution of how much an emissions scenario, or its warming signal, directly or indirectly modifies a single AR event (e.g., strengthening of landfalling AR IVT) or long-term trend in the AR climatology (e.g., shifts in landfalling AR latitude). A different approach looks at past and future global temperature-based scenarios over a shorter time period, rather than centennial-long, transient emissions-based scenarios, in part inspired by the reformulation of climate policy within the Paris Climate Agreement (Hannart et al., 2016; Stott et al., 2016; Mitchell et al., 2017; Stone et al., 2019). These temperature scenarios run over more targeted time periods after emissions have peaked and stabilized permit the usage of atmospheric climate models of high spatial resolution, thus better resolving the AR filaments and their landfall lifecycle.

To the best of our knowledge, little to no research has been conducted to date in studying landfalling AR character and frequency using stabilized warming experiments. This is a major research gap as ARs have been shown to be both constructive and destructive to water resource management based on their landfall duration and maximum intensity reached (Ralph et al., 2019). In fact, a third of all droughts in the western United States (US) have been ended by an increase in landfall AR activity (Dettinger, 2013), most recently in 2017 (Ullrich et al., 2018). However, ARs have also accounted for the vast majority (84%) of flood damages in the western US with 13 AR events accounting for more than half of the total damages (Corringham et al., 2019). As evidenced by various modeling strategies, more destructive AR events will occur more regularly in a warmer world (Gao et al., 2015; Shields and Kiehl, 2016; Gershunov et al., 2019; Huang et al., 2020; Rhoades et al., 2020b). Yet, these studies are likely upper-bound estimates on shifts in AR characteristics as they only assess the highest commonly simulated emission scenario. Given that global climate policy now explicitly intends to avoid a high-temperature (and hence high-emissions) future, a more nuanced analysis of the shifts in AR character with systematic warming is needed.

In this study, we aim to address these literature gaps. We do this by leveraging an ensemble of high-resolution Community Earth System Model simulations performed under stabilized warming scenarios (Bacmeister et al., 2014; Wehner, 2014; Wehner, 2014) and a recently developed AR lifecycle tracking workflow (Rhoades et al., 2020a, 2020b). By combining these approaches, we are able to isolate how landfalling AR characteristics in the western US differ between a world that might have been (i.e. with no historical anthropogenic emissions) from the world that is (i.e., with anthropogenic emissions). In addition, we evaluate how three future stabilized warming scenarios of +1.5 °C, +2.0 °C, and +3.0 °C influence AR character and frequency. To make this work more useable for stakeholder communities, we employ the recently developed Ralph et al. (2019) AR impacts category scale that relates AR characteristics (i.e., maximum IVT and AR duration) to water management outcomes. Lastly, we build upon the work of Corringham et al. (2019) in characterizing historic flood-related damages from ARs to show how future changes in AR character could lead to dramatically increased flood damages.

The paper proceeds as follows: in section 2, we discuss the methods used to investigate the effects of global warming on AR characteristics including the AR tracking algorithm, AR impacts scale, and the statistical methods employed. Section 3 presents the results of our analysis. Section 4 provides a discussion on potential limitations of our study and how our results compare with the broader literature. Section 5 summarizes the major findings of our analysis.

2. Methods

2.1. Earth system model simulations

The atmosphere and land components of the Community Earth System Model (CESM) version 1 are used in our experiments (Hurrell et al., 2013). More specifically, the atmospheric component is the Community Atmosphere Model version 5.3 with the finite-volume dynamical core (CAM5.3-FV (Neale et al., 2010)) and the land component is the Community Land Model version 4 (CLM4.0 (Oleson et al., 2010)). The horizontal resolution of the simulations are 0.23 °x 0.31° with 30 vertical levels. The physics timestep is set to 900 s with 18× as many dynamics timesteps. Further details on these simulations, including sub-grid-scale parameterizations, are provided in (Wehner, 2014).

2.2. Stabilized warming scenarios

The Climate of the 20th Century Plus Detection and Attribution (C20C+ D&A) project seeks to understand natural climate variability, particularly in the atmosphere, and changes to this variability due to anthropogenic emissions (Stone et al., 2019). To do this, standard experimental protocols are set (e.g., prescribed ocean conditions, standardized climate forcings, common historical time-periods and outputs, etc.) and utilized by a broad-number of Earth system modeling groups to better isolate cause and effect. Within the C20C+ D&A, broadly, there are two simulation types: natural historical (Nat-Hist) and all historical (All-Hist). All-Hist simulations are run under observed historical climate forcings, including anthropogenic greenhouse gases, aerosol burdens, stratospheric ozone, solar luminosity, monthly sea surface temperatures (SSTs), and monthly sea ice coverage (SIC). Nat-Hist simulations are run under year-1855 anthropogenic forcings, and naturalized versions of the All-Hist SSTs and SIC. For Nat-Hist, the All-Hist observed SSTs are cooled according to a spatially, seasonally, and interannually-varying attributable warming pattern based on the anthropogenic warming in an ensemble of coupled atmosphere-ocean climate models, while the SIC is advanced through a delta method based on the attributable warming (Stone and Pall, 2021). In each of the CESM simulations used in this study, the simulations are spun-up from their initial conditions over the first simulated year prior to inclusion into the analysis. This is done to ensure, in particular, that atmosphere-land feedbacks are in equilibrium (e.g., soil moisture feedback). For this analysis, we use all five ensemble members from Nat-Hist and All-Hist. However we only use the simulated years that span 2006–2015 and leave out simulated years 1996–2005. Additionally, because of corrupted output files we only use

complete-year simulations which provided 3-hourly specific humidity and meridional and zonal winds which are used to compute integrated vapor transport (IVT) to track ARs. This resulted in 31 and 45 total simulated years for Nat-Hist and All-Hist, respectively.

In response to the realignment of global climate change policy toward temperature thresholds, the Half a Degree Additional Warming, Prognosis and Projected Impacts (HAPPI) project proposed a series of experiments similar to the C20C+ D&A experiments, but for warmer worlds anticipated in the future (Mitchell et al., 2017). The intent of the HAPPI experiments is to isolate the societal implications of global warming up to +1.5 °C (HAPPI1.5) and +2.0 °C (HAPPI2.0) from pre-industrial conditions, particularly on extreme weather events. Given the usefulness of a "world averted" counterfactual for diagnosing the benefits of the Paris Agreement warming limits, another HAPPI simulation of +3.0 °C (the so-called UNHAPPI3.0 experiment) was developed. The HAPPI1.5, HAPPI2.0, and UNHAPPI3.0 experiments all take analogous 2006–2015 boundary conditions, yet simulate the conditions with deltas derived from stabilized near-surface air temperatures of +1.55 °C, +2.05 °C, and +3.05 °C at end-century. HAPPI1.5 uses RCP2.6 radiative forcings and SST deltas based on the circa year-2100 warming in an ensemble of coupled atmosphere-ocean model simulations driven by the RCP2.6 emissions scenario. HAPPI2.0 follows HAPPI1.5, but with CO_2 concentrations and SSTs adjusted using the linear combination of two ensembles of coupled atmosphere-ocean model simulations, forced by the RCP2.6 and RCP4.5 emissions scenarios respectively, in order to obtain an additional 0.5 °C of warming. UNHAPPI3.0 in turn adjusts CO_2 concentrations and SSTs by following the linear combination of ensembles forced by the RCP4.5 and RCP8.5 emissions scenarios in order to obtain an additional 1.0 °C of warming. SICs for the HAPPI1.5 and HAPPI2.0 experiments are adjusted for consistency with SSTs, while UNHAPPI3.0 maintains HAPPI2.0 SICs. A consequence of this experiment design is that the climate response moving from the approximately +0.5 °C between All-Hist to HAPPI1.5 is different than the response moving the same amount from HAPPI1.5 to HAPPI2.0, due to the different balance of greenhouse gas and non-greenhouse gas forcings involved (Wehner et al., 2018a). More details about the high-resolution CESM simulations used in this study and their application to investigating shifts in tropical cyclone characteristics can be found in Wehner et al. (2018b) and, more broadly, across the multi-model ensemble of HAPPI simulations to investigate shifts in heat extremes in Wehner et al. (2018a). With similar constraints as Nat-Hist and All-Hist we are able to use 57, 57, and 49 simulated years from HAPPI1.5, HAPPI2.0, and UNHAPPI3.0, respectively.

2.3. Atmospheric river tracking

To isolate ARs that make landfall along the coastline of the western US, we employ the TempestExtremes AR tracking algorithm (Ullrich and Zarzycki, 2017; Ullrich et al., 2021). Customized TempestExtremes algorithm choices in SplineARs (i.e., min area of 25, size laplacian of 35, min val of 250, min laplacian of 50,000, min abslat of 15) and StitchBlobs (i.e., min time of 16 and min size of 35) were chosen for this study. These parameters were chosen based on the horizontal-resolution (0.25°) and 3-hourly outputs of the C20C+ D&A and HAPPI experiments. As discussed in Rhoades et al. (2020a) several extensions were made to TempestExtremes that enable AR path tracking and diagnostics of the AR events from their origin through landfall (Table 1). Once ARs make landfall, we then employ more recent TempestExtremes extensions (discussed in Rhoades et al. (2020b)) to identify the societal impacts of AR events using a recently developed AR impacts category scale (Ralph et al., 2019), herein called AR Cats. AR Cats, analogous to the Saffir–Simpson hurricane category scale, were designed to more clearly relay the societal impacts of landfalling ARs, particularly how beneficial or hazardous they are to water resource management. Specifically, AR Cats relate maximum IVT, which correlates with maximum precipitation rates, with AR duration, which correlates with storm-total precipitation. Importantly, these AR Cats also have been shown to correlate well with flood insurance damages on a logarithmic scale (Corringham et al., 2019).

2.4. Bayesian geospatial analysis of AR counts

Using a Bayesian framework, we employ a geospatial statistics methodology to cast our AR counts derived from the ensemble of high-resolution CESM simulations into a probability distribution. This is done to more formally characterize uncertainty due to issues with the number of simulated years and signal-to-noise issues of warming on landfalling AR characteristics (e.g., return periods for Cat 4 and 5 AR events).

For each warming scenario and AR category, the input data for this analysis is the AR counts for each year at each CESM grid cell over Washington, Oregon, and California. At each grid cell, we statistically model the counts in each year arising from a Poisson distribution, which is a discrete probability distribution that specifies the likelihood of a given number of "events" (here, AR occurrence) in a fixed time interval (here, each year). The Poisson distribution is determined by a single statistical parameter, often denoted λ, which in this case specifies the average number of ARs for each AR Cat per year at each grid cell. A

Table 1
Coastal western US AR characteristics under global warming conditions of +0 °C (Nat-Hist), +0.85 °C (All-Hist), +1.5 °C (HAPPI1.5), +2.0 °C (HAPPI2.0) and +3.0 °C (UNHAPPI3.0) with 95% confidence intervals. Annual counts represent the average number of ARs over the entire North Pacific (Latitude: 15N–60N, Longitude: 120E to 100W) each year. Annual landfall counts represent the annual average number of ARs that make landfall anywhere in the coastal western US for at least one timeslice. Total lifetime is the average AR lifetime from origin in the North Pacific through terminus in the coastal western US. Lifetime gridcell count is the average total number of gridcells impinged upon by an AR from its origin in the North Pacific through terminus in the coastal western US over the total lifetime of the AR. Landfall duration is the average landfall duration of an AR from the first landfall timeslice in the coastal western US through termination. Landfall maximum IVT is the average maximum IVT value reached at any gridcell of the coastal western US over an AR landfall duration. AR category is the average Ralph et al. (2019) AR category reached within the impacts scale across all landfalling ARs. Landfall interval is the annual average interval between AR landfalls anywhere within the coastal western US. Back-to-back AR landfalls are the annual average number of coastal western US AR landfalls within one week of one another.

Stabilized Warming Scenario	Number of years	Annual Count	Annual Land fall Count	Total *Lifetime* (*Days*)	Lifetime *Grid−Cell*	Land fall *Duration* (*Days*)	*Land fall Maximum IVT* (*kg/m/s*)	*AR* Category	*Land fall Interval* (*Days*)	*Back to Back AR Land falls* (*One − Week*)
+0 °C	31	137 ± 4	38 ± 2	5.1 ± 0.1	28,300 ± 1430	0.7 ± 0.06	762 ± 18	1.80 ± 0.10	21.5 ± 1.5	8 ± 1
+0.85 °C	45	132 ± 2	41 ± 2	5.3 ± 0.1	33,400 ± 1160	0.7 ± 0.05	776 ± 11	1.95 ± 0.08	21.1 ± 1.7	8 ± 1
+1.5 °C	57	134 ± 2	43 ± 2	5.5 ± 0.1	36,200 ± 1280	0.8 ± 0.04	806 ± 12	2.06 ± 0.08	19.0 ± 1.1	10 ± 1
+2 °C	57	133 ± 2	44 ± 2	5.6 ± 0.1	37,900 ± 1280	0.8 ± 0.05	823 ± 13	2.19 ± 0.07	18.8 ± 1.1	10 ± 1
+3 °C	49	131 ± 3	48 ± 3	5.9 ± 0.1	43,900 ± 1600	0.9 ± 0.05	858 ± 16	2.38 ± 0.09	18.1 ± 1.3	11 ± 1

useful quantity that can be derived using λ is the probability of experiencing at least one AR of a given AR Cat per year, defined as $P_{\geq 1}$:

$$\text{Prob(at least 1 AR per year)} \equiv P_{\geq 1} = 1 - e^{-\lambda}.$$

This probability can be converted to a return period by taking its inverse; in this case, the return period corresponds to the average number of years it will take for a grid cell to experience at least one AR event of a specific AR Cat.

Given the spatial structure of ARs and their spatial coherence in landfall locations (i.e., if a grid cell experiences an AR, a neighboring grid cell is more likely to also experience an AR), we assign the spatial field of rate parameters a prior distribution that explicitly incorporates spatial autocorrelation. Specifically, we use a hybrid version of the conditionally autoregressive (CAR) prior distribution for the natural logarithm of λ. The CAR distribution, which is a natural prior for gridded climate model output, models the natural logarithm of λ as a spatially-dependent random effect (Banerjee et al., 2004; Pascutto et al., 2000) wherein λ at a particular grid cell is conditionally independent of all other grid cells given the values in neighboring grid cells. However, to more flexibly model the spatial dependence in the AR count data, we use a hybrid version of the CAR prior (Leroux et al., 2000) in which the precision matrix of the random effects is a convex combination of the CAR precision matrix and a spatially-independent precision matrix; note that the popular intrinsic CAR prior (Rue and Held, 2005) is a special case of this statistical model. The final component of our Bayesian hierarchical model is a prior distribution on the hyperparameters of the hybrid CAR distribution; here, we simply use flat, noninformative prior distributions in all cases. For each warming scenario and AR category group, we then use Markov chain Monte Carlo methods to draw samples from the posterior distribution of the rate parameters. These samples are used to calculate the posterior mean of the average number of ARs per year, the probability of experiencing at least one AR per year (i.e., $P_{\geq 1}$), and the return period of this probability as well as quantify all statistical uncertainties. For the map indicating differences in $P_{\geq 1}$ across warming scenarios, we use stippling to indicate grid cells where the 99% credible interval of the difference does not include zero (i.e., equivalent to the "virtually certain" uncertainty condition outlined in the Intergovernmental Panel on Climate Change (Mastrandrea et al., 2010)).

2.5. Analysis of shift in annual AR flood damages with warming

To estimate the shift in annual AR flood damages with warming, we leverage historical western US AR flood damage estimates provided by Corringham et al., 2019. Our analysis consists of the following steps: (1) fit a statistical distribution to the observed damages for each AR category, match the boxplot summary statistics provided in Corringham et al. (2019); (2) use the All-Hist as a baseline, calculate the percent change in the annual AR counts by category from the simulations; and (3) apply these percent changes to the historical annual AR counts and resample the cost distributions with these modified counts.

For the first step of the analysis, given the extremely heavy tail of the flood damage cost distributions from Corringham et al. (2019) (see Table 3), we opted to fit a skew-t distribution to the log of the percentiles, specifically the 25th, 50th, 62.5th, 75th, 85th, and 95th percentiles. Analogous to Corringham et al. (2019), lower bounds of the skew-t distributions are bounded between $10 thousand dollars per event (Cat 1-3) to $5 billion dollars per event (Cat 5). We constrain our upper bounds on the skew-t distributions for each AR Cat distribution to three-fourths the distance between the 95th percentile and maximum value. This choice ensures that our estimates are not heavily influenced by sampling an extreme outlier event and yields the best match with the observed cost distributions in Corringham et al. (2019) (i.e., comparable annual average flood damages of $1.1 billion). Using the fitted skew-t distributions from above, for each of 1000 Monte Carlo replicates we conducted the following steps:

1. For AR category $k = 1, \ldots, 5$, draw n_k values from the fitted distribution corresponding to the kth category, where n_k is the number of observed ARs from Corringham et al. (2019) in category k from the full 40 year period. This sampling accounts for the upper and lower bounds on the category-specific cost distributions as described above.
2. For each category, sum the n_k values and divide by 40. This represents the total damages from Cat k ARs over the 40 years.
3. Finally, sum the total damages from all AR categories to arrive at a total damages from all ARs per year.

Using this approach, the Monte Carlo average damages per year is estimated to be $1.06 billion, with a 95% confidence interval of ($762 million, $1.41 billion), which is comparable to the estimates provided in Corringham et al. (2019) (Figure S1).

Next, we use a percent-based bias correction procedure on the AR frequencies to update our AR flood damage estimates. As described above, using the All-Hist counts as a baseline, we first calculate the percent change in the annual AR counts by category. For reference, the number of ARs in each category for each warming scenario per year and the percent changes in AR counts relative to All-Hist are given in Table 2. Applying these multiplicative changes to the number of ARs in each category per year from Corringham et al. (2019), we then multiply by 100 to end up with an estimated number of ARs per 100 years. Note that we multiply by 100 years, instead of the 40 year period used in Corringham et al. (2019), in order to avoid issues associated with rounding. Again, using the fitted skew-t distributions for each of 1000 Monte Carlo replicates and for each warming experiment, we conduct a similar sampling scheme as described above. The resulting Monte Carlo samples are used to estimate the average total flood damages from ARs per year in each warming experiment along with 95% Monte Carlo based uncertainty intervals.

3. Results

We first isolate how each stabilized warming scenario influences AR characteristics from their origin in the North Pacific through landfall in the coastal western US. Table 1 summarizes annual average AR lifecycle characteristics across the C20C+ D&A and HAPPI experiments. The lifetime size and the life cycle duration of an AR increases by 15% and 6 h per ° C, respectively. These two AR characteristic changes with warming are in line with well-established thermodynamic feedbacks to ARs enabling them to be larger and more long-lived (Payne et al., 2020). In addition, a notable, steady increase in the annual average number of western US landfalling ARs is seen from +0 °C (38 ARs/year) to +3 °C (48 ARs/year) at a rate of +3 landfalling ARs per °C per year. Important to AR related impacts, landfalling ARs reach higher average max IVT values of +30 kg/m/s per °C and longer average durations of +3 h per °C. The net result is an increase in the average AR Cat reached from +0 °C (1.8) to +3 °C (2.4), which correlates with an increase in maximum precipitation rate and/or storm-total precipitation (Ralph et al., 2019). Similar to results found in Rhoades et al. (2020b), a decrease in the annual average interval between western US landfalling ARs is found from +0 °C (21.5 days) to +3 °C (18.0 days) and, more specifically, +1 AR per °C per year occurs within one-week of another. Back-to-back AR events that occur within one-to-two weeks of one another are particularly impactful to water resource managers as they precondition the land-surface to generate amplified and abrupt runoff and can stress-test flood pool assumptions built into reservoir operation (Hatchett et al., 2020; Henn et al., 2020; Sumargo et al., 2020).

Estimates provided in the previous paragraph include all coastal western US landfalling ARs, yet the Ralph et al. (2019) AR impacts scale provides a means to better translate their potential in being either beneficial or hazardous to water resource managers. Figure S2 shows all of the tracked coastal western US landfalling AR events simulated by the C20C+ D&A and HAPPI experiments overlain on the Ralph et al. (2019)

Table 2
Monte Carlo based annual average estimated flood damages from coastal western US landfalling ARs (millions of dollars) across the C20C+ D&A and HAPPI experiments with 95% confidence intervals (best estimate provided along with the lower and upper bound in parantheses). The total AR frequency, as shown in Fig. 1, is computed as the annual average total AR landfalls within any of the coastal western US states that meet, at least, a category (Cat) 1 on the Ralph et al. (2019) AR impacts scale. Percents relative to +0.85 °C (All-Hist) are included in parentheses.

Stabilized Warming Scenario	Annual Average Damages	Total AR Frequency	Cat 1 AR Frequency	Cat 2 AR Frequency	Cat 3 AR Frequency	Cat 4 AR Frequency	Cat 5 AR Frequency
+0 °C	$1040 ($852-$1240)	19.1 (93.3%)	11.3 (99.7%)	6.1 (88.0%)	1.3 (74.4%)	0.5 (127%)	0.1 (62.2%)
+0.85 °C	$1070 ($890-$1270)	20.5 (100%)	11.4 (100%)	6.9 (100%)	1.8 (100%)	0.4 (100%)	0.2 (100%)
+1.5 °C	$1820 ($1560-$2090)	21.7 (106%)	10.6 (93.6%)	7.8 (113%)	2.4 (136%)	0.8 (237%)	0.1 (90.2%)
+2 °C	$2080 ($1800-$2360)	21.9 (107%)	9.6 (84.5%)	8.4 (122%)	2.9 (165%)	0.9 (262%)	0.2 (124%)
+3 °C	$3250 ($2900-$3600)	23.6 (115%)	9.6 (84.3%)	8.9 (129%)	3.3 (186%)	1.5 (413%)	0.5 (328%)

AR impacts scale. Fig. 1 shows only landfalling ARs that met at least a Cat 1 on the Ralph et al. (2019) AR impacts scale normalized by the number of simulated years used from each experiment. A steady increase in the number of landfalling ARs per year that reach, at least, Cat 1 is seen from +0 °C (19.1/year) to +3 °C (23.6/year) with ARs more regularly occupying a more hazardous role to water resource management. Cat 1-2 events, "mostly to primarily beneficial" to water resource management, represent 91% of all ARs at +0 °C and at +3 °C this decreases to 78% of all ARs. Conversely, a steady uptick in Cat 3 events, "balance of beneficial and hazardous" to water resource management, occurs. In a world of +0–0.85 °C, Cat 3 AR events make up 7-9% of all AR events, whereas in a +2-3 °C future these events occupy 13-14%, respectively. Worryingly, Cat 4-5 events, "mostly to primarily hazardous" to water resource management, occupy 2% of all landfalling AR events at +0–0.85 °C, steadily increase to 4-5% at +1.5–2 °C and reach 8% at +3 °C. The seasonality of coastal western US landfalling AR totals are also sensitive to warming. Fig. 2 shows the average number of landfalling ARs across each month of the water year binned by the maximum AR Cat reached. The most active months of AR activity across C20C+ D&A and HAPPI experiments is in November through January. However, at +0 °C a more distinguished peak in AR activity is seen in December (4/year) compared with other months (3/year in November and January and 2/year in the shoulder months). Comparatively, +0.85 °C increases average AR activity in November, January and February (>12/year). This increase in wintertime AR activity is maintained at +1.5 through +3 °C, yet ARs more frequently reach higher AR Cats with increased warming.

To assess how warming influences coastal AR activity and character differently across the coastal western US we present spatial distributions of the posterior mean of the rate of ARs (number per year) in Fig. 3, obtained from the geospatial analysis described in Section 2.4. A clear and systematic increase in the number of landfalling ARs per year is seen in the Pacific Northwest with each +1 °C of warming. In particular, shifts in the inland penetration of ARs is particularly pronounced in Washington and Oregon. More specifically, a +2-3 °C of warming ensures that there is a >90% probability that an AR will impinge upon every portion of the state each year (Figure S3). Further the probability of, at least, one Cat 3 and 4-5 AR making landfall anywhere along the coast of Oregon and Washington each year is doubled from +0 °C to +3 °C with yearly odds increased to >1/3 and >1/6, respectively. An increase in AR probability from +0.85 °C to +2-3 °C is significant over the entire coastal western US for AR Cat 1-2 and the coastal regions of Oregon and

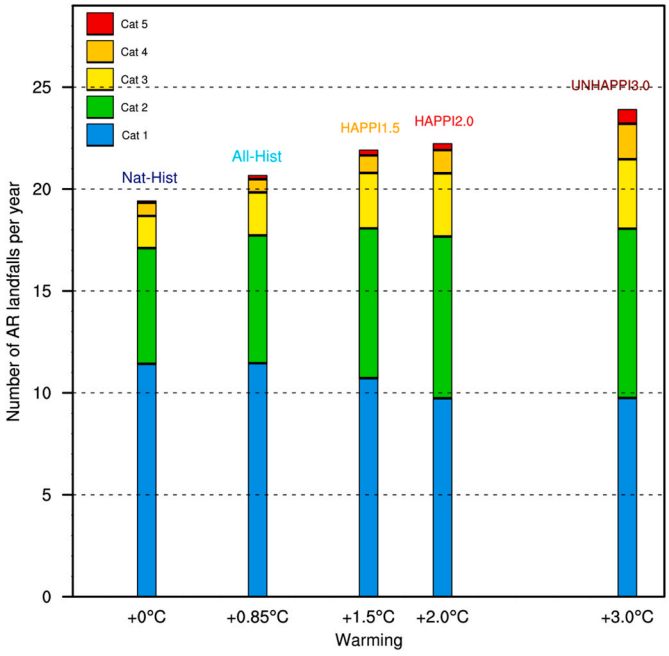

Fig. 1. Annual average totals of coastal western US landfalling AR events simulated by each of the C20C+ D&A and HAPPI experiments. Each AR is binned by the maximum Ralph et al. (Ralph et al., 2019) category reached. Histograms are labeled by C20C+ D&A and HAPPI experiment name and spaced on the x-axis according to their average global temperature delta from the Nat-Hist experiment. AR frequencies are also summarized in Table 2.

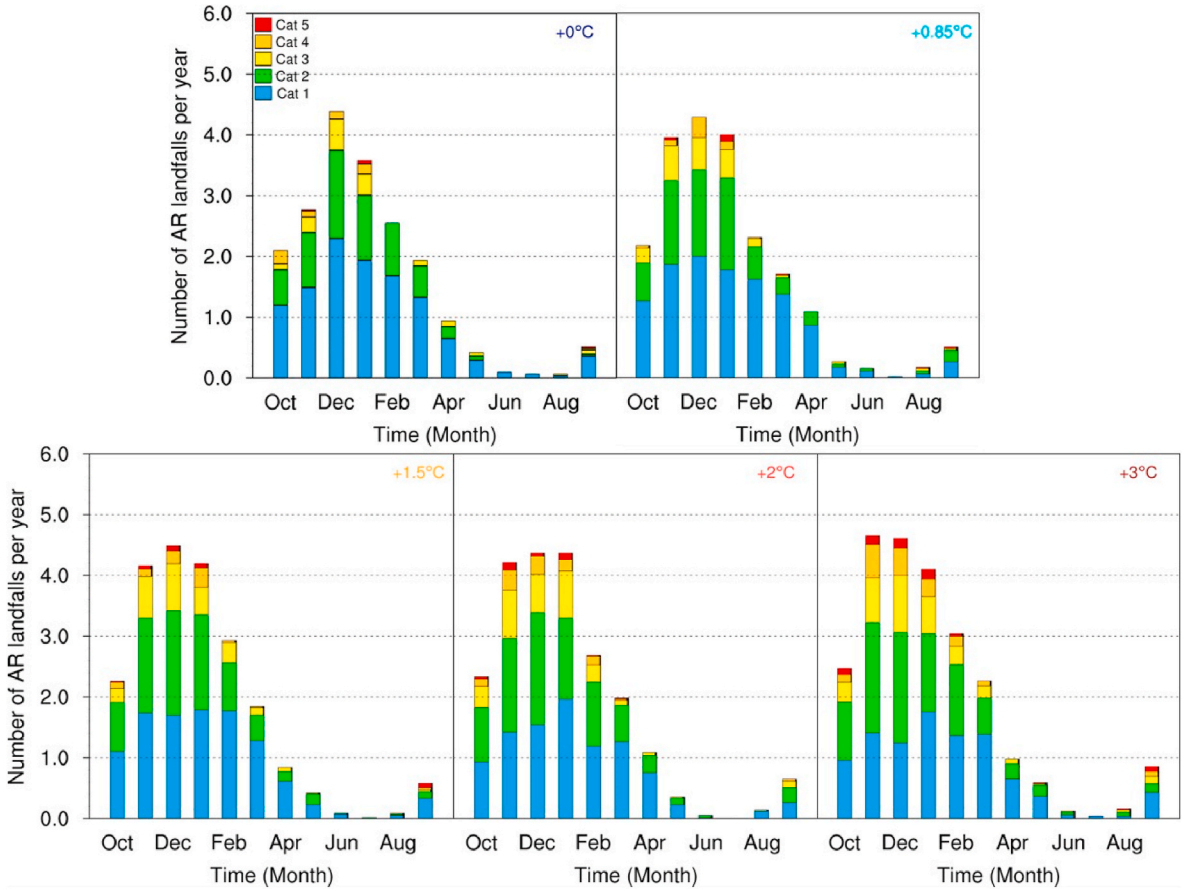

Fig. 2. Monthly average totals of coastal western US landfalling AR events simulated by each of the C20C+ D&A and HAPPI experiments and binned by the maximum Ralph et al., 2019 AR category reached. Each plot is labeled by the average global temperature delta from the Nat-Hist experiment.

Washington for AR Cats 3-5 (Supplemental Figure S4). The systematic influence of warming on AR landfalls over California is less clear than the Pacific Northwest, particularly in Cat 3-5 ARs. This is likely indicative that more simulated years are needed to better isolate the signal of warming from the noise of natural variability as the rate of higher Cat ARs in California is more infrequent than the Pacific Northwest.

To more clearly quantify how warming influences the bulk frequency of AR landfalls from the lens of water resource management, we now discuss return period shifts across C20C+ and HAPPI experiments. Generally, return periods across AR Cats decrease with warming. At +3 °C of warming it is nearly assured that every portion of the coastal western US will be impacted by an AR each year (i.e., average return period is nearly one). In addition, more hazardous ARs become considerably more frequent. Cat 3 AR return periods decrease by ~3 years with warming from +0 to 2 °C and at +3 °C become a 1-in-10 year event. Cat 4-5 ARs also become much more frequent with warming, but, importantly, have a noisier signal. This is because higher return period events are further out into the tail of the assumed Poisson distribution (see Methods section for more details) and therefore more sensitive to the number of simulated years (i.e., 30-60 years across experiments). With that said, from +0 to 3 °C Cat 4-5 AR events shift from approximately a 1-in-50 or 1-in-100 year event to approximately a 1-in-25 year event.

As shown in the seminal work of Corringham et al. (2019) western US landfalling ARs generate, on average, flood damages amounting to $1.1 billion per year. Importantly, annual average flood damages are closely tied with the occurrence of Cat 4-5 ARs as these events have an order of magnitude higher cost than Cat 1-2 ARs. Therefore, any shift in the frequency of higher Cat ARs with warming disproportionately influences AR flood damage totals. Fig. 4 and Table 2 provide AR frequency changes across AR Cats and the resultant flood damage totals for each of the C20C+ D&A and HAPPI experiments. A notable increase in average AR flood damages of $1 billion per year per °C of warming is shown. From +0 °C to +0.85 °C, an increase of $30 million per year is associated with +1 AR per year, namely Cat 2-3 ARs. However, from +0.85 °C to +2 °C a near doubling of annual average AR damages (+$1.04 billion) is found. This is due to an uptick in the number of ARs per year (+1.5/year), particularly Cat 3-5 ARs. From +0.85 °C to +3 °C AR frequency increases by +3.1/year and Cat 4-5 frequency increases by 413% and 328%, respectively. This results in a tripling of annual average flood damages from +0.85 °C ($1.07 billion/year) to +3 °C ($3.25 billion/year).

4. Discussion

Before we discuss our major findings, we first highlight potential uncertainties in our analysis and their broader implications. First, we utilize a single-model ensemble to assess shifts in landfalling AR character. Therefore, there may be model dependent uncertainties in our CESM simulations that may influence AR characteristics (e.g., maximum IVT reached) and frequency. For example, Hagos et al. (2015), Gao et al. (2015), and Hagos et al. (2016) have all shown that there are systematic CESM biases related to higher AR frequencies associated with an erroneous equatorward position of the subtropical jet in November–March (NDJFM). We note a brief analysis in this study that indicates our CESM simulations have similar biases, namely higher NDJFM geopotential heights in the northwest Pacific and an amplified IVT climatology near 20N in the All-Hist simulation relative to the ERA5 reanalysis dataset (Copernicus Climate Change, 2017) (left column of Figure S5). The influences of warming on NDJFM IVT tracks and relation to the

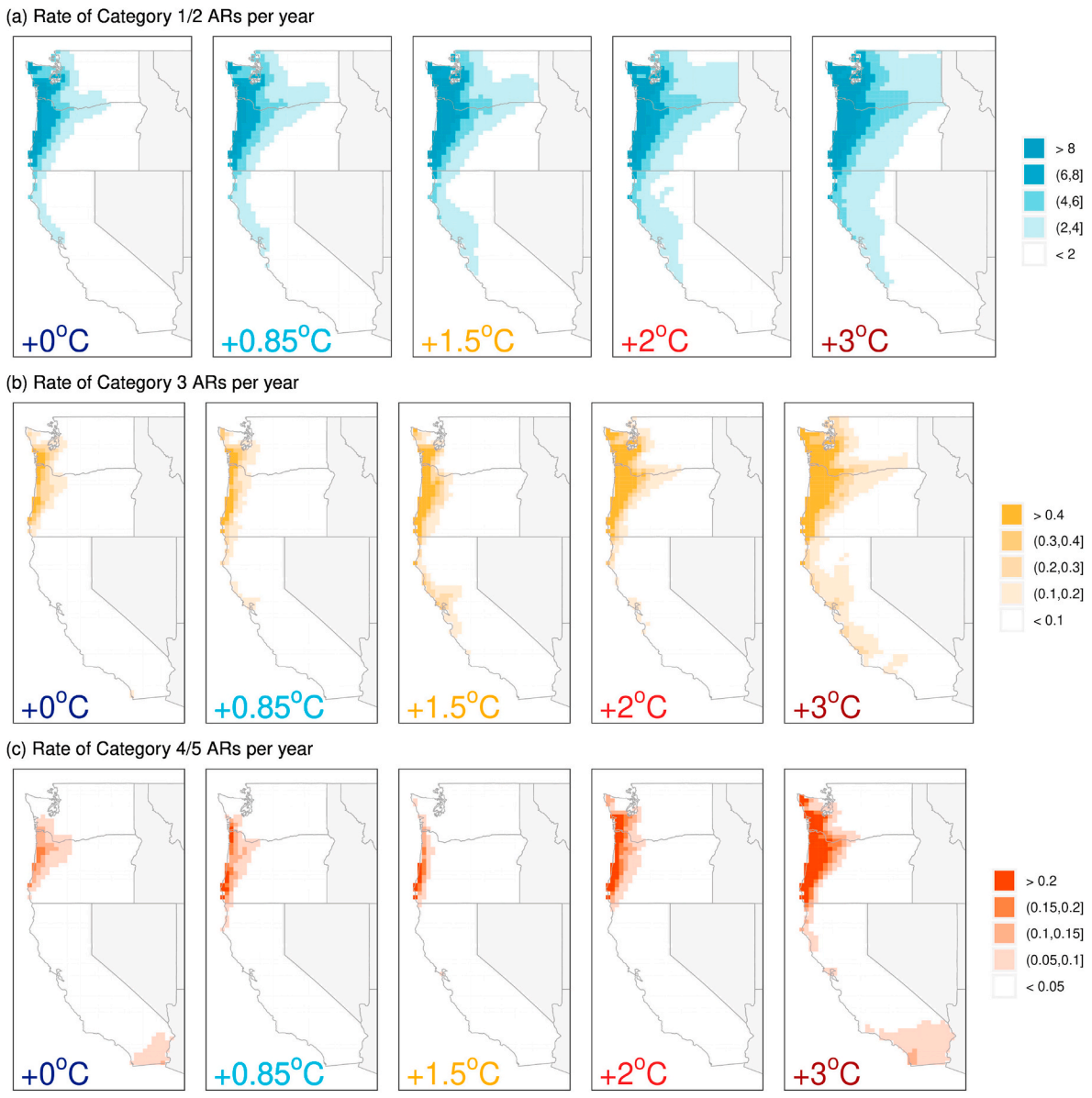

Fig. 3. Spatial distributions of the posterior mean of statistical estimates for coastal western US landfalling AR events per year derived from C20C+ D&A and HAPPI simulations. Per year landfalling AR estimates are combined according to their qualitative water management designations in the Ralph et al., 2019 AR category scale in a) Cat 1-2 "mostly or primarily beneficial", b) Cat 3 "balance between beneficial and hazardous", and c) Cat 4-5 "mostly or primarily hazardous". Plots are labeled by each C20C+ and HAPPI experiment's average global temperature delta from the Nat-Hist experiment.

subtropical jet was also briefly analyzed by comparing the UNHAPPI3.0 and All-Hist experiments (right column of Figure S5). UNHAPPI3.0 was chosen as it has the largest warming signal of all HAPPI experiments and would most clearly indicate any subtropical jet position change that might then influence the NDJFM IVT climatology. We note that UNHAPPI3.0 compared with All-Hist has IVT fields that are generally larger throughout the North Pacific and, in particular, at higher latitudes. Although the IVT field presents a mixture of both the thermodynamical (e.g., Clausius-Clapeyron) and dynamical (e.g., storm tracks and/or subtropical jet shift) effects of warming, this may indicate that the subtropical jet does move northward in a $+3\,^{\circ}C$ future enhancing IVT transport in northern latitudes (although this is beyond the scope of the current study to definitively confirm).

Another example of CESM specific biases was discussed in Reed et al. (2015) who showed that CESM run with the Community Atmosphere Model with the Finite Volume (CAM-FV) versus the Spectral Element (CAM-SE) dynamical core has shown important influences on the number and intensity of tropical cyclones (i.e., CAM-FV produces less and weaker tropical cyclones than CAM-SE). Although the All-Hist experiments in this study were run with slightly different sub-grid-scale parameterizations and time periods than Rhoades et al. (2020a) and Rhoades et al. (2020b), there is qualitative evidence that CAM-FV produces a smaller number of Cat reaching ARs per year than CAM-SE too, in particular less Cat 4-5 ARs. However, even though CAM-FV may produce less total Cat reaching ARs per year in the All-Hist experiment (20.5 ARs/year) than the CAM-SE based results in Rhoades et al. (2020b) (24.7 ARs/year) the counts more align with estimates found in the ERA5 reanalysis dataset in that study (19.5 ARs/year). The important caveat is the number of Cat 4-5 landfalling ARs in the All-Hist simulations (0.4 ARs/year) are, at least, half as frequent as in ERA5 (0.9 ARs/year) and in Ralph et al. (2019) (0.9 ARs/year) and Corringham et al. (2019) (2.8 ARs/year) who used the MERRA-2 and NCEP-NCAR reanalyses, respectively. However, as mentioned in the Methods section, we utilize a percent-bias adjustment in AR counts to

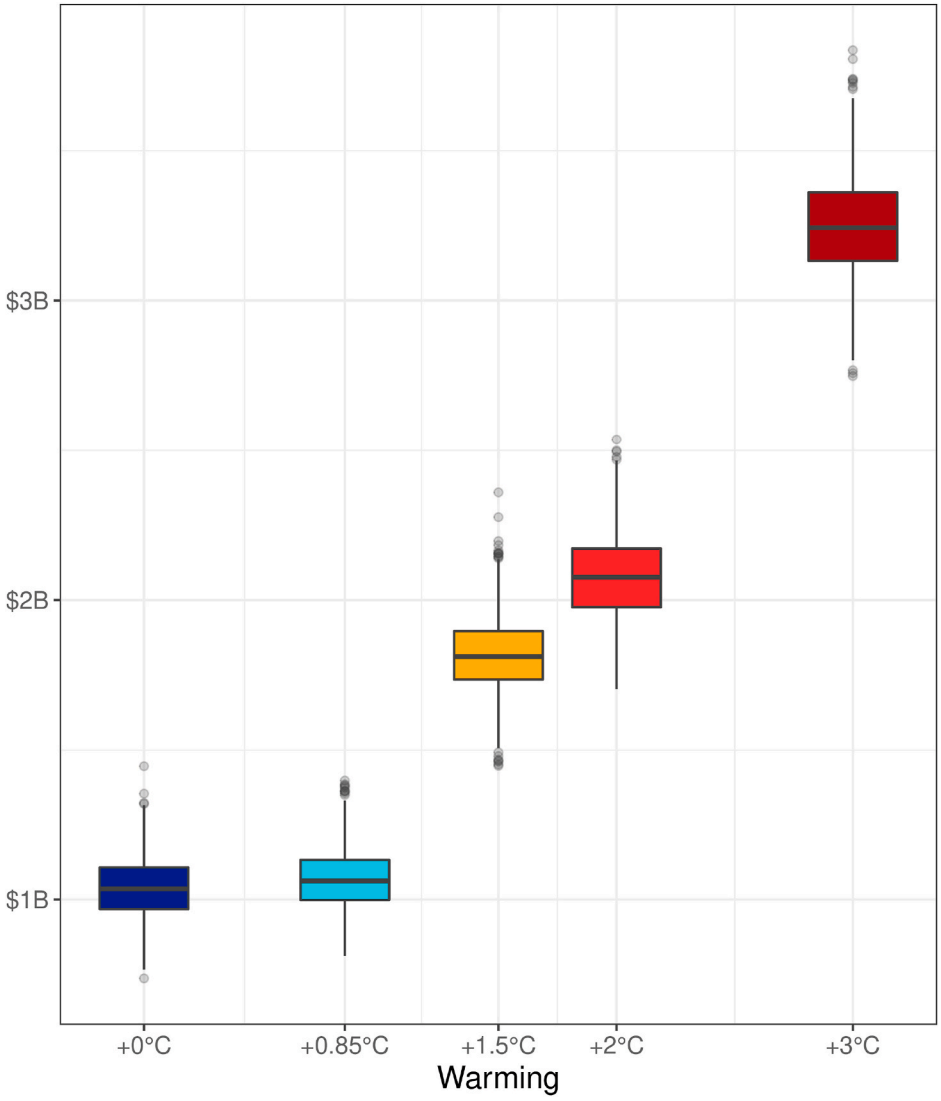

Fig. 4. Annual AR flood damage estimates based on Markov chain Monte Carlo sampling of the C20C+ D&A and HAPPI experiments. Box-and-whisker plots are labeled on the *x*-axis according to each C20C+ D&A and HAPPI experiment's average global temperature delta from the Nat-Hist experiment. Box-and-whiskers indicate the 5th to 95th percentiles with the 25th percentile, median, and 75th percentile demarcating the box region. Flood damage outliers outside of the 5th and 95th percentiles are shown via dots.

account for potential CAM-FV biases in the All-Hist experiment relative to Corringham et al. (2019). Since we use a single model in this study we assume that this bias correction will consistently address uncertainty across other C20C+ D&A and HAPPI experiments. Therefore, given the aforementioned assumption holds, our flood damages estimates should be robust to any model related AR biases.

Additionally, although the uniform high-resolution (0.25°) CESM simulations used in this study are representative of the cutting-edge in Earth system models (Haarsma et al., 2016) they may still be insufficient in resolving all local effects of landfalling ARs. Specifically, the simulations may not resolve the topographic complexity of the western US coastal mountain ranges which in turn could influence the inland penetration of ARs and the maximum AR Cat reached in these regions due to less water vapor being translated into precipitation. This particular source of uncertainty is partly why we isolate our analysis to the three westernmost states of the US.

Further, we use a single AR tracker in this study. The Tempest-Extremes AR tracker is known to be more restrictive than other AR tracking algorithms (Shields et al., 2018; Rutz et al., 2019; O'Brien et al., 2020). Therefore, in contrast to the previously mentioned uncertainty, our results may underestimate the area, inland penetration, and the duration of landfalling ARs. However, it was recently shown that AR algorithm choice has little influence on landfalling ARs that reach higher AR Cats (Zhou et al., 2020). As a result, we do not foresee our choice of AR algorithm significantly influencing our estimated AR flood damage estimates as they are primarily driven by the most hazardous events. Although AR algorithm choice may have a limited influence on AR Cat 4 and 5 event counts, we do note that some of the discrepancies in systematic warming effects on AR Cat 4 and 5 frequencies in Fig. 3, particularly in southern California, may have been due to the need for larger sample sizes of simulated years across experiments to get clearer statistical convergence in AR Cat 4 and 5 frequencies with warming. We also note that the AR flood damages discussed in Corringham et al. (2019) are dependent on the spatial distribution of population and infrastructure, and in particular how those relate to the spatial distribution of hazards such as floods. This spatial dependence of AR landfall near flood-prone infrastructure is not accounted for in our economic analysis.

Importantly, some of the simulated years in the C20C+ D&A and HAPPI experiments were left out of our analysis due to experimental design decisions. For example, we only use historical (2006-2015) and future (2106-2115) time periods that overlap to eliminate potential confounding factors of climate variability, arising via the imposed ocean conditions, on AR characteristics. Therefore, in Nat-Hist and All-Hist we do not use the simulated years of 1996–2005 in our analysis because they are not included in the HAPPI simulations. Similarly, we only use a simulated year as long as the components needed to compute 3-hourly IVT estimates are provided for an entire simulated year. This results in

9 of 40 years, 5 of 50 years, 3 of 60 years, 3 of 60 years, and 1 of 60 years left out of our analysis for Nat-Hist, All-Hist, HAPPI1.5, HAPPI2.0, and UNHAPPI3.0, respectively, because of corrupt output files. Additionally, based on the experimental design of the HAPPI simulations (i.e., future recreations of 2006–2015) we may not account for the full spectrum of climate modes of variability and their interactions with AR activity and intensity. For example, the El Niño Longitude Index shows that 2006–2015 had seven La Niña events (weak-to-strong), two neutral events, and one El Niño event (weak) (Patricola et al., 2019). As a result our study does not explicitly account for the effects of moderate-to-strong El Niño events on ARs.

5. Conclusions

Our study provides several important findings. First, an important shift in total counts of coastal western US landfalling ARs with warming is shown (+3 landfalling ARs per °C per year). This is likely due to ARs becoming larger (+15% lifetime area per °C) and more long-lived (+6 h per °C) over the North Pacific with warming. The societal importance of this is made more apparent when ARs are binned by their Ralph et al. (2019) AR impact scale category. We show that ARs generally become less beneficial and more hazardous to water resource management with warming. In fact, the most hazardous AR events (Cat 4-5) increase from 2% of all events at +0–0.85 °C to 8% at +3 °C. In other words, at +3 °C Cat 3 ARs shift from approximately a 1-in-30 year event to a <1-in-10 year event and Cat 4-5 ARs shift from approximately a 1-in-100 year event to approximately a 1-in-25 year event. The warming induced shift has a clearer signal-to-noise in Washington and Oregon than it does in California, likely due to issues of simulation sample size. Therefore, we likely need more than the ~30-60 simulated years available from by the experiments used in this study to make definitive conclusions about how warming influences higher Cat ARs in subregions of the coastal western US, particularly southern California. Yet, even with these limitations, we show that shifts in Cat 3-5 AR event return periods at +3 °C will certainly stress-test current infrastructure and water management practices. This is because infrastructure has historically only been designed using historically observed events (e.g., 1-in-100 year events) under an assumption of stationarity. However, operational lifetime of infrastructure is often a half-century or more due to funding and regulatory restraints. For example, two-thirds of dams in California are, at least, 50 years old (Escriva-Bou et al., 2019). The increase in regularity of hazardous ARs will also be compounded by the fact that back-to-back ARs become more frequent with warming too (+1 AR per °C per year occurs within one-week of another). The combination of the aforementioned findings results in significantly higher flood damages with warming across coastal western US states. In fact, we find a 3× increase in the annual average flood damages from +0 °C ($1.04 billion/year) to +3 °C ($3.25 billion/year). All together, we show the potential societal and economic ramifications of inaction on climate mitigation (e.g., Paris Climate Agreement) to limit global warming to +2 °C.

It is important to note that there is still ample time to limit global warming to below +3 °C. Yet, even an increase of +0.5 °C from present day is projected to increase coastal western US flood damages by +$750 million/year (+70% from 2006 to 2015 rates). Notably, our flood damage estimates have been bias-corrected for model inconsistencies compared with historical reanalysis data from Corringham et al. (2019), yet these estimates do not account for factors such as societal innovation nor compounding effects in the future. Innovations that may diminish the impact of more frequent hazardous ARs in a warmer world include alterations to water management practices such as forecast informed reservoir operation (Delaney et al., 2020), climate change informed engineering design criteria such as intensity-duration-frequency and/or depth-area-duration curves (Srivastava et al., 2019), and more permeable and less flood-prone infrastructure design (Enzi et al., 2017). Compounding effects that could lead to enhanced damages include aging water infrastructure that are in operation beyond their intended lifetimes (Saleh, 2019), continued conurbation in flood prone regions (Mount, 2017) and alterations to the frequency of rain-instead-of-snow and/or rain-on-snow events (Hatchett et al., 2020; Henn et al., 2020), particularly in headwater regions of reservoirs that have variable freezing levels (Chen et al., 2019; Sumargo et al., 2020).

Data availability

The computed IVT files and coastal western US landfalling AR masks from the C20C+ D&A and HAPPI simulation can be found via a NERSC Science Gateway - https://portal.nersc.gov/archive/home/a/arhoades/Shared/www/WCE_2020.

CRediT authorship contribution statement

Alan M. Rhoades: Conceptualization, Methodology, Formal analysis, Writing – original draft, Visualization. **Mark D. Risser:** Conceptualization, Methodology, Formal analysis, Writing – original draft, Visualization, Funding acquisition. **Dáithí A. Stone:** Methodology, Data curation, Writing – review & editing. **Michael F. Wehner:** Methodology, Data curation, Writing – review & editing. **Andrew D. Jones:** Conceptualization, Funding acquisition, Writing – review & editing, Supervision.

Declaration of competing interest

The authors declare that they have no known competing financial interests or personal relationships that could have appeared to influence the work reported in this paper.

Acknowledgements

The authors would like to first acknowledge Tom Corringham and another anonymous reviewer for their insightful and constructive feedback during the review process. We would also like to acknowledge our major funding sources including the Office of Biological and Environmental Research of the U.S. Department of Energy. Authors Rhoades, Risser, and Wehner were funded by the Regional and Global Climate Modeling Program (RGCM) program under "the Calibrated and Systematic Characterization, Attribution and Detection of Extremes (CASCADE)" Science Focus Area (award no. DE-AC02- 05CH11231) and Jones and Rhoades were funded by the "A Framework for Improving Analysis and Modeling of Earth System and Intersectoral Dynamics at Regional Scales" project (award no. DE-SC0016605). Author Stone contributed under the Whakahura project funded by the Aotearoa New Zealand Ministry of Business, Innovation and Employment's Endeavour Fund. Analysis and model simulations were performed using the National Energy Research Scientific Computing Center (NERSC), specifically Cori-Haswell and Cori-KNL supercomputing facilities (contract number DE-AC02-05CH11231).

Appendix A. Supplementary data

Supplementary data to this article can be found online at https://doi.org/10.1016/j.wace.2021.100326.

References

Allan, R.P., Barlow, M., Byrne, M.P., Cherchi, A., Douville, H., Fowler, H.J., Gan, T.Y., Pendergrass, A.G., Rosenfeld, D., Swann, A.L.S., Wilcox, L.J., Zolina, O., 2020. Advances in understanding large-scale responses of the water cycle to climate change. Ann. N. Y. Acad. Sci. https://doi.org/10.1111/nyas.14337.

Allen, M.R., Ingram, W.J., 2002. Constraints on future changes in climate and the hydrologic cycle. Nature 419, 228–232. https://doi.org/10.1038/nature01092.

Bacmeister, J.T., Wehner, M.F., Neale, R.B., Gettelman, A., Hannay, C., Lauritzen, P.H., Caron, J.M., Truesdale, J.E., 2014. Exploratory high-resolution climate simulations using the community atmosphere model (CAM). J. Clim. 27, 3073–3099. https://doi.org/10.1175/JCLI-D-13-00387.1.

Banerjee, S., Carlin, B.P., Gelfand, A.E., 2004. Hierarchical Modeling and Analysis for Spatial Data, Monographs on Statistics and Applied Probability. Chapman & Hall, London.

Chen, X., Leung, L.R., Wigmosta, M., Richmond, M., 2019. Impact of atmospheric rivers on surface hydrological processes in western U.S. Watersheds. J. Geophys. Res.: Atmospheres 124, 8896–8916. https://doi.org/10.1029/2019JD030468.

Copernicus Climate Change Service Climate Data Store (CDS), Copernicus Climate Change Service (C3S): ERA5: Fifth GenEration of ECMWF Atmospheric Reanalyses of the Global Cli- Mate, 2017. https://cds.climate.copernicus.eu/cdsapp%23!/dataset/reanalysis-era5-pressure-levels?tab=overview.

Corringham, T.W., Ralph, F.M., Gershunov, A., Cayan, D.R., Talbot, C.A., 2019. Atmospheric rivers drive flood damages in the western United States. Sci. Adv. 5 https://doi.org/10.1126/sciadv.aax4631.

Delaney, C.J., Hartman, R.K., Mendoza, J., Dettinger, M., Delle Monache, L., Jasperse, J., Ralph, F.M., Talbot, C., Brown, J., Reynolds, D., Evett, S., 2020. Forecast informed reservoir operations using ensemble streamflow predictions for a multipurpose reservoir in northern California. Water Resour. Res. 56, e2019WR026604 https://doi.org/10.1029/2019WR026604, e2019WR026604 2019WR026604.

Dettinger, M., 2011. Climate change, atmospheric rivers, and floods in california – a multimodel analysis of storm frequency and magnitude changes. JAWRA J. Am. Water Resour. Assoc. 47, 514–523. https://doi.org/10.1111/j.1752-1688.2011.00546.x.

Dettinger, M.D., 2013. Atmospheric rivers as drought busters on the U.S. West coast. J. Hydrometeorol. 14, 1721–1732. https://doi.org/10.1175/JHM-D-13-02.1.

Dettinger, M.D., Ralph, F.M., Das, T., Neiman, P.J., Cayan, D.R., 2011. Atmospheric rivers, floods and the water resources of California. Water 3, 445–478. https://doi.org/10.3390/w3020445.

Dirmeyer, P.A., Brubaker, K.L., 2007. Characterization of the Global Hydrologic Cycle from a Back-Trajectory Analysis of Atmospheric Water Vapor. J. Hydrometeorol. 8, 20–37. https://doi.org/10.1175/JHM557.1.

Enzi, V., Cameron, B., Dezsényi, P., Gedge, D., Mann, G., Pitha, U., 2017. Nature-Based Solutions and Buildings – the Power of Surfaces to Help Cities Adapt to Climate Change and to Deliver Biodiversity. Springer International Publishing, Cham, pp. 159–183.

Escriva-Bou, A., Mount, J., Jezdimirovic, J., 2019. Dams in California. Public Policy Institute of California. http://www.ppic.org/publication/water-use-in-california/.

Fish, M.A., Wilson, A.M., Ralph, F.M., 2019. atmospheric river families: definition and associated synoptic conditions. J. Hydrometeorol. 20, 2091–2108. https://doi.org/10.1175/JHM-D-18-0217.1.

Gao, Y., Lu, J., Leung, L.R., Yang, Q., Hagos, S., Qian, Y., 2015. Dynamical and thermodynamical modulations on future changes of landfalling atmospheric rivers over western North America. Geophys. Res. Lett. 42, 7179–7186. https://doi.org/10.1002/2015GL065435.

Gershunov, A., Shulgina, T., Clemesha, R.E., Guirguis, K., Pierce, D.W., Dettinger, M.D., Lavers, D.A., Cayan, D.R., Polade, S.D., Kalansky, J., et al., 2019. Precipitation regime change in western North America: the role of atmospheric rivers. Sci. Rep. 9, 1–11. https://doi.org/10.1038/s41598-019-46169-w.

Gimeno, L., Nieto, R., Vázquez, M., Lavers, D., 2014. Atmospheric rivers: a mini–review. Front. Earth Sci. 2, 2. https://doi.org/10.3389/feart.2014.00002.

Gonzales, K.R., Swain, D.L., Nardi, K.M., Barnes, E.A., Diffenbaugh, N.S., 2019. Recent warming of landfalling atmospheric rivers along the west coast of the United States. J. Geophys. Res.: Atmospheres 124, 6810–6826. https://doi.org/10.1029/2018JD029860.

Haarsma, R.J., Roberts, M.J., Vidale, P.L., Senior, C.A., Bellucci, A., Bao, Q., Chang, P., Corti, S., Fučkar, N.S., Guemas, V., von Hardenberg, J., Hazeleger, W., Kodama, C., Koenigk, T., Leung, L.R., Lu, J., Luo, J.-J., Mao, J., Mizielinski, M.S., Mizuta, R., Nobre, P., Satoh, M., Scoccimarro, E., Semmler, T., Small, J., von Storch, J.-S., 2016. High resolution model intercomparison project (HighResMIP v1.0) for CMIP6. Geosci. Model Dev. (GMD) 9, 4185–4208. https://doi.org/10.5194/gmd-9-4185-2016.

Hagos, S., Leung, L.R., Yang, Q., Zhao, C., Lu, J., 2015. Resolution and Dynamical core dependence of atmospheric river frequency in global model simulations. J. Clim. 28, 2764–2776. https://doi.org/10.1175/JCLI-D-14-00567.1.

Hagos, S.M., Leung, L.R., Yoon, J.-H., Lu, J., Gao, Y., 2016. A projection of changes in landfalling atmospheric river frequency and extreme precipitation over western North America from the Large Ensemble CESM simulations. Geophys. Res. Lett. 43, 1357–1363. https://doi.org/10.1002/2015GL067392.

Hannart, A., Pearl, J., Otto, F.E.L., Naveau, P., Ghil, M., 2016. Causal counterfactual theory for the attribution of weather and climate-related events. Bull. Am. Meteorol. Soc. 97, 99–110. https://doi.org/10.1175/BAMS-D-14-00034.1.

Hatchett, B.J., Cao, Q., Dawson, P.B., Ellis, C.J., Hecht, C.W., Kawzenuk, B., Lancaster, J. T., Osborne, T.C., Wilson, A.M., Anderson, M.L., Dettinger, M.D., Kalansky, J.F., Kaplan, M.L., Let- tenmaier, D.P., Oakley, N.S., Ralph, F.M., Reynolds, D.W., White, A.B., Sierks, M., Sumargo, E., 2020. Observations of an extreme atmospheric river storm with a diverse sensor network. Earth Space Sci. 7, e2020EA001129 https://doi.org/10.1029/2020EA001129.

Held, I.M., Soden, B.J., 2006. Robust responses of the hydrological cycle to global warming. J. Clim. 19, 5686–5699. https://doi.org/10.1175/JCLI3990.1.

Henn, B., Musselman, K.N., Lestak, L., Ralph, F.M., Molotch, N.P., 2020. Extreme runoff generation from atmospheric river driven snowmelt during the 2017 oroville dam spillways incident. Geophys. Res. Lett. 47, e2020GL088189 https://doi.org/10.1029/2020GL088189.

Huang, X., Swain, D.L., Hall, A.D., 2020. Future precipitation increase from very high resolution ensemble downscaling of extreme atmospheric river storms in California. Sci. Adv. 6 https://doi.org/10.1126/sciadv.aba1323.

Hurrell, J.W., Holland, M.M., Gent, P.R., Ghan, S., Kay, J.E., Kushner, P.J., Lamarque, J.-F., Large, W.G., Lawrence, D., Lindsay, K., Lipscomb, W.H., Long, M.C., Mahowald, N., Marsh, D.R., Neale, R.B., Rasch, P., Vavrus, S., Vertenstein, M., Bader, D., Collins, W.D., Hack, J.J., Kiehl, J., Marshall, S., 2013. The community Earth system model: a framework for collaborative research. Bull. Am. Meteorol. Soc. 94, 1339–1360. https://doi.org/10.1175/BAMS-D-12-00121.1.

Kim, H.-M., Zhou, Y., Alexander, M.A., 2019. Changes in atmospheric rivers and moisture transport over the Northeast Pacific and western North America in response to ENSO diversity. Clim. Dynam. 52, 7375–7388. https://doi.org/10.1007/s00382-017-3598-9.

Lamjiri, M.A., Dettinger, M.D., Ralph, F.M., Oakley, N.S., Rutz, J.J., 2018. Hourly analyses of the large storms and atmospheric rivers that provide most of California's precipitation in only 10 to 100 hours per year. San Franc. Estuary Watershed Sci. 16 https://doi.org/10.15447/sfews.2018v16iss4art1.

Leroux, B.G., Lei, X., Breslow, N., 2000. Estimation of Disease Rates in Small Areas: A New Mixed Model for Spatial Dependence. Springer New York, New York, NY, pp. 179–191. https://doi.org/10.1007/978-1-4612-1284-3_4.

Mastrandrea, M.D., Field, C.B., Stocker, T.F., Edenhofer, O., Ebi, K.L., Frame, D.J., Held, H., Kriegler, E., Mach, K.J., Matschoss, P.R., et al., 2010. Guidance Note for Lead Authors of the IPCC Fifth Assessment Report on Consistent Treatment of Uncertainties, Intergovernmental Panel on Climate Change. http://www.ipcc.ch.

Mitchell, D., AchutaRao, K., Allen, M., Bethke, I., Beyerle, U., Ciavarella, A., Forster, P. M., Fuglestvedt, J., Gillett, N., Haustein, K., Ingram, W., Iversen, T., Kharin, V., Klingaman, N., Massey, N., Fischer, E., Schleussner, C.-F., Scinocca, J., Seland, Ø., Shiogama, H., Shuckburgh, E., Sparrow, S., Stone, D., Uhe, P., Wallom, D., Wehner, M., Zaaboul, R., 2017. Half a degree additional warming, prognosis and projected impacts (HAPPI): background and experimental design. Geosci. Model Dev. (GMD) 10, 571–583. https://doi.org/10.5194/gmd-10-571-2017.

Mount, J., 2017. Floods in California. Public Policy Institute of California. https://www.ppic.org/publication/floods-in-california/.

Neale, R.B., Chen, C.-C., Gettelman, A., Lauritzen, P.H., Park, S., Williamson, D.L., Conley, A.J., Garcia, R., Kinnison, D., Lamarque, J.-F., Marsh, D., Mills, M., Smith, A. K., Tilmes, S., Vitt, F., Cameron-Smith, P., Collins, W.D., Iacono, M.J., Easter, R.C., Liu, X., Ghan, S.J., Rasch, P.J., Taylor, M.A., 2010. Description of the {NCAR}{C} ommunity {A}tmosphere {M}odel ({CAM} 5.0), NCAR Tech- Nical Note NCAR/TN-486+STR. National Center for Atmospheric Research, Boulder, Colorado. http://www.cesm.ucar.edu/models/cesm1.0/cam/docs/description/cam5_desc.pdf.

Newell, R.E., Newell, N.E., Zhu, Y., Scott, C., 1992. Tropospheric rivers? – a pilot study. Geophys. Res. Lett. 19, 2401–2404. https://doi.org/10.1029/92GL02916.

O'Brien, T.A., Wehner, M.F., Payne, A.E., Shields, C.A., Rutz, J.J., Ruby Leung, L., Martin Ralph, F., Marquardt Collow, B., Allison, Guan, B., Lora, J.M., McClenny, E., Nardi, K.M., Ramos, A.M., Tomé, R., Sarangi, C., Shearer, E.J., Ullrich, P., Zarzycki, C.M., Loring, B., Huang, H., Díaz, H.A.I., Rhoades, A.M., Zhou, Y., 2020. Increases in future AR count and size: overview of the ARTMIP tier 2 CMIP5/6 experiment. Earth and Space Science Open Archive ESSOAr. https://search.proquest.com/docview/2451144564? accountid=14496.

Oleson, K., Lawrence, D., Bonan, G., Flanner, M., Kluzek, E., Lawrence, P., Levis, S., Swenson, S., Thornton, P., Dai, A., Decker, M., Dickinson, R., Feddema, J., Heald, C., Hoffman, F., Lamarque, J., Mahowald, N., Niu, G., Qian, T., Randerson, J., Running, S., Sakaguchi, K., Slater, A., Stockli, R., Wang, A., Yang, Z., Zeng, X., Zeng, X., 2010. Technical Description of Version 4.0 of the Community Land Model (CLM), NCAR Technical Note NCAR/TN-478+STR. National Center for Atmospheric Research, Boulder, Colorado.

Pascutto, C., Wakefield, J., Best, N., Richardson, S., Bernardinelli, L., Staines, A., Elliott, P., 2000. Statistical issues in the analysis of disease mapping data. Stat. Med. 19, 2493–2519. https://doi.org/10.1002/1097-0258(20000915/30)19:17/18<2493::AID-SIM584>3.0.CO;2-D.

Patricola, C.M., O'Brien, J.P., Risser, M.D., Rhoades, A.M., O'Brien, T.A., Ullrich, P.A., Stone, D.A., Collins, W.D., 2019. Maximizing enso as a source of western us hydroclimate predictability. Clim. Dynam. 1–22. https://doi.org/10.1007/s00382-019-05004-8.

Payne, A.E., Magnusdottir, G., 2014. Dynamics of landfalling atmospheric rivers over the north pacific in 30 Years of MERRA reanalysis. J. Clim. 27, 7133–7150. https://doi.org/10.1175/JCLI-D-14-00034.1.

Payne, A.E., Demory, M.-E., Leung, L.R., Ramos, A.M., Shields, C.A., Rutz, J.J., Siler, N., Villarini, G., Hall, A., Ralph, F.M., 2020. Responses and impacts of atmospheric rivers to climate change. Nat. Rev. Earth Environ. 1, 143–157. https://doi.org/10.1038/s43017-020-0030-5.

Prein, A.F., Pendergrass, A.G., 2019. Can we constrain uncertainty in hydrologic cycle projections? Geophys. Res. Lett. 46, 3911–3916. https://doi.org/10.1029/2018GL081529.

Ralph, F.M., Dettinger, M., Lavers, D., Gorodetskaya, I.V., Martin, A., Viale, M., White, A. B., Oakley, N., Rutz, J., Spackman, J.R., Wernli, H., Cordeira, J., 2017. Atmospheric rivers emerge as a global science and applications Focus. Bull. Am. Meteorol. Soc. 98, 1969–1973. https://doi.org/10.1175/BAMS-D-16-0262.1.

Ralph, F.M., Dettinger, M.D., Cairns, M.M., Galarneau, T.J., Eylander, J., 2018. Defining "atmospheric river": how the glossary of meteorology helped resolve a debate. Bull. Am. Meteorol. Soc. 99, 837–839. https://doi.org/10.1175/BAMS-D-17-0157.1.

Ralph, F.M., Rutz, J.J., Cordeira, J.M., Dettinger, M., Anderson, M., Reynolds, D., Schick, L.J., Smallcomb, C., 2019. A scale to characterize the strength and impacts of atmospheric rivers. Bull. Am. Meteorol. Soc. 100, 269–289. https://doi.org/10.1175/BAMS-D-18-0023.1.

Reed, K.A., Bacmeister, J.T., Rosenbloom, N.A., Wehner, M.F., Bates, S.C., Lauritzen, P. H., Truesdale, J.E., Hannay, C., 2015. Impact of the dynamical core on the direct simulation of tropical cyclones in a high-resolution global model. Geophys. Res. Lett. 42, 3603–3608. https://doi.org/10.1002/2015GL063974.

Rhoades, A.M., Jones, A.D., O'Brien, T.A., O'Brien, J.P., Ullrich, P.A., Zarzycki, C.M., 2020a. Influences of North Pacific ocean domain extent on the western U.S. Winter hydroclimatology in variable-resolution CESM. J. Geophys. Res.: Atmospheres 125, e2019JD031977. https://doi.org/10.1029/2019JD031977.

Rhoades, A.M., Jones, A.D., Srivastava, A., Huang, H., O'Brien, T.A., Patricola, C.M., Ullrich, P.A., Wehner, M., Zhou, Y., 2020b. The shifting scales of western u.s. landfalling atmospheric rivers under climate change. Geophys. Res. Lett. 47, e2020GL089096 https://doi.org/10.1029/2020GL089096.

Rue, H., Held, L., 2005. Gaussian Markov Random Fields: Theory and Applications, Volume 104 of Monographs on Statistics and Applied Probability. Chapman & Hall, London.

Rutz, J.J., Shields, C.A., Lora, J.M., Payne, A.E., Guan, B., Ullrich, P., O'Brien, T., Leung, L.R., Ralph, F.M., Wehner, M., Brands, S., Collow, A., Goldenson, N., Gorodetskaya, I., Griffith, H., Kashinath, K., Kawzenuk, B., Krishnan, H., Kurlin, V., Lavers, D., Magnusdottir, G., Mahoney, K., McClenny, E., Muszynski, G., Nguyen, P. D., Prabhat, M., Qian, Y., Ramos, A.M., Sarangi, C., Sellars, S., Shulgina, T., Tome, R., Waliser, D., Walton, D., Wick, G., Wilson, A.M., Viale, M., 2019. The atmospheric river tracking method intercomparison project (ARTMIP): quantifying uncertainties in atmospheric river climatology. J. Geophys. Res.: Atmospheres 124, 13777–13802. https://doi.org/10.1029/2019JD030936.

Saleh, F., 2019. Climate change and infrastructure resilience. In: Frontiers of Engineering: Reports on Leading-Edge Engineering from the 2018 Symposium. National Academies Press. https://www.ncbi.nlm.nih.gov/books/NBK538707/.

Shields, C.A., Kiehl, J.T., 2016. Atmospheric river landfall-latitude changes in future climate simulations. Geophys. Res. Lett. 43, 8775–8782. https://doi.org/10.1002/2016GL070470.

Shields, C.A., Rutz, J.J., Leung, L.-Y., Ralph, F.M., Wehner, M., Kawzenuk, B., Lora, J.M., McClenny, E., Osborne, T., Payne, A.E., Ullrich, P., Gershunov, A., Goldenson, N., Guan, B., Qian, Y., Ramos, A.M., Sarangi, C., Sellars, S., Gorodetskaya, I., Kashinath, K., Kurlin, V., Mahoney, K., Muszynski, G., Pierce, R., Subramanian, A.C., Tome, R., Waliser, D., Walton, D., Wick, G., Wilson, A., Lavers, D., Prabhat, Collow, A., Krishnan, H., Magnusdottir, G., Nguyen, P., 2018. atmospheric river tracking method intercomparison project (ARTMIP): project goals and experimental design. Geosci. Model Dev. (GMD) 11, 2455–2474. https://doi.org/10.5194/gmd-11-2455-2018.

Srivastava, A., Grotjahn, R., Ullrich, P.A., Risser, M., 2019. A unified approach to evaluating precipitation frequency estimates with uncertainty quantification: application to Florida and California watersheds. J. Hydrol. 578, 124095. https://doi.org/10.1016/j. jhydrol.2019.124095.

Stone, D.A., Pall, P., 2021. Benchmark estimate of the effect of anthropogenic emissions on the ocean surface. Int. J. Climatol. 1–17. https://doi.org/10.1002/joc.7002 n/a.

Stone, D.A., Christidis, N., Folland, C., Perkins-kirkpatrick, S., Perlwitz, J., Shiogama, H., Wehner, M.F., Wolski, P., Cholia, S., Krishnan, H., Murray, D., Angélil, O., Beyerle, U., Ciavarella, A., Dittus, A., Quan, X.-w., Tadross, M., Berkeley, L., 2019. Experiment design of the international CLIVAR C20C+ detection and attribution project. Weather Clim. Extr. 24, 100206. https://doi.org/10.1016/j. wace.2019.100206.

Stott, P.A., Christidis, N., Otto, F.E.L., Sun, Y., Vanderlinden, J.-P., van Oldenborgh, G.J., Vautard, R., von Storch, H., Walton, P., Yiou, P., Zwiers, F.W., 2016. Attribution of extreme weather and climate-related events. WIREs Clim. Chang. 7, 23–41. https://doi.org/10.1002/wcc.380.

Sumargo, E., Cannon, F., Ralph, F.M., Henn, B., 2020. Freezing level fore-cast error can consume reservoir flood control storage: potentials for lake oroville and new bullards bar reservoirs in California. Water Resour. Res. 56, e2020WR027072 https://doi.org/10.1029/2020WR027072.

Thackeray, C.W., DeAngelis, A.M., Hall, A., Swain, D.L., Qu, X., 2018. On the connection between global hydrologic sensitivity and regional wet extremes. Geophys. Res. Lett. 45 https://doi.org/10.1029/2018GL079698, 11,343–11,351.

Trenberth, K.E., Dai, A., Rasmussen, R.M., Parsons, D.B., 2003. The changing character of precipitation. Bull. Am. Meteorol. Soc. 84, 1205–1218. https://doi.org/10.1175/BAMS-84-9-1205.

Ullrich, P.A., Zarzycki, C.M., 2017. TempestExtremes: a framework for scale-insensitive pointwise feature tracking on unstructured grids. Geosci. Model Dev. (GMD) 10, 1069–1090. https://doi.org/10.5194/gmd-10-1069-2017.

Ullrich, P.A., Xu, Z., Rhoades, A., Dettinger, M., Mount, J., Jones, A., Vahmani, P., 2018. California's drought of the future: a midcentury recreation of the exceptional conditions of 2012–2017. Earth's Future 6, 1568–1587. https://doi.org/10.1029/2018EF001007.

Ullrich, P.A., Zarzycki, C.M., McClenny, E.E., Pinheiro, M.C., Stansfield, A.M., Reed, K.A., 2021. TempestExtremes v2.1: a community framework for feature detection, tracking and analysis in large datasets. Geosci. Model Dev. Discuss. (GMDD) 2021, 1–37. https://doi.org/10.5194/gmd-2020-303.

Wehner, M., Stone, D., Mitchell, D., Shiogama, H., Fischer, E., Graff, L.S., Kharin, V.V., Lierhammer, L., Sanderson, B., Krishnan, H., 2018a. Changes in extremely hot days under stabilized 1.5 and 2.0 C global warming scenarios as simulated by the HAPPI multi-model ensemble. Earth Syst. Dynam. 9, 299–311. https://doi.org/10.5194/esd-9-299-2018.

Wehner F, Michael, K. A. Reed, F. Li, Prabhat, J. Bacmeister, C.-T. Chen, C. Paciorek, P. J. Gleckler, K. R. Sperber, W. D. Collins, A. Gettelman, C. Jablonowski, 2014. The effect of horizontal resolution on simulation quality in the Community Atmospheric Model, CAM5.1. Journal of Advances in Modeling Earth Systems 6, 980–997. https://doi.org/10.1002/2013MS000276.

Wehner, M.F., Reed, K.A., Loring, B., Stone, D., Krishnan, H., 2018b. Changes in tropical cyclones under stabilized 1.5 and 2.0 C global warming scenarios as simulated by the Community Atmospheric Model under the HAPPI protocols. Earth Syst. Dynam. 9, 187–195. https://doi.org/10.5194/esd-9-187-2018.

Zhou, Y., Kim, H., Guan, B., 2018. Life cycle of atmospheric rivers: identification and climatological characteristics. J. Geophys. Res.: Atmospheres 123. https://doi.org/10.1029/2018JD029180, 12,715–12,725.

Zhou, Y., O'brien, T., Ullrich, P., Collins, W., Patricola, C., Rhoades, A., 2020. Uncertainties in atmospheric river life cycles by detection algorithms: climatology and variability. Earth Space Sci. Open Arch. 43. https://doi.org/10.1002/essoar.10504174.1.